Surface chemistry and morphology of the solid electrolyte interphase on silicon nanowire lithium-ion battery anodes

Candace K. Chan [a], Riccardo Ruffo [b], Seung Sae Hong [c], Yi Cui [d],*

[a] Department of Chemistry, Stanford University, Stanford, CA 94305, United States
[b] Department of Materials Science, University of Milano-Bicocca, Milan, Italy
[c] Department of Applied Physics, Stanford University, Stanford, CA 94305, United States
[d] Department of Materials Science and Engineering, Stanford University, 476 Lomita Mall, Stanford, CA 94305, United States

ABSTRACT

Silicon nanowires (SiNWs) have the potential to perform as anodes for lithium-ion batteries with a much higher energy density than graphite. However, there has been little work in understanding the surface chemistry of the solid electrolyte interphase (SEI) formed on silicon due to the reduction of the electrolyte. Given that a good, passivating SEI layer plays such a crucial role in graphite anodes, we have characterized the surface composition and morphology of the SEI formed on the SiNWs using X-ray photoelectron spectroscopy (XPS) and scanning electron microscopy (SEM). We have found that the SEI is composed of reduction products similar to that found on graphite electrodes, with Li_2CO_3 as an important component. Combined with electrochemical impedance spectroscopy, the results were used to determine the optimal cycling parameters for good cycling. The role of the native SiO_2 as well as the effect of the surface area of the SiNWs on reactivity with the electrolyte were also addressed.

© 2009 Elsevier B.V. All rights reserved.

1. Introduction

Lithium-ion batteries have become the most important rechargeable battery for portable electronics and electric and plug-in hybrid electric vehicles [1], with high energy density materials being of considerable interest. Numerous replacements for the graphite anode have been investigated, with silicon [2–7] being one of the most attractive since its high theoretical specific capacity of 4200 mAh g^{-1} is more than 10 times larger than graphite (372 mAh g^{-1}) [8].

Because the negative electrode operates at low potentials close to metallic lithium, the electrolyte is outside its thermodynamic stability region. In addition, electrochemical reduction of both the solvent and salt of the electrolyte can cause the formation of a film on the surface of the anode. This film is composed of insoluble reduction products of the electrolyte. The presence of this film, called the solid electrolyte interphase (SEI), has been known to be an important feature of graphite anodes that allows for reversible cycling and long term stability due to surface passivation [9–11]. The components of the SEI on graphite electrodes have been well studied and have shown that the decomposition products of the ethylene carbonate solvent, namely lithium alkyl carbonates and lithium carbonate, dominate the SEI layer [12–15].

However, little attention has been directed towards understanding the surface chemistry and SEI formation in silicon anodes. The first charge profile of Si when it is reacted with Li is characterized by a flat plateau at about 0.1 V vs. Li. Between 1.0 and 0.2 V vs. Li/Li$^+$, the potential region where the SEI formation in graphite is known to occur, there is often very little capacity. This has caused some to report that there is no SEI formation on the Si electrode [3]. However, because the cell is operating at the potential where the organic electrolyte is thermodynamically unstable [16], we can still expect the decomposition of the electrolyte to form some kind of an SEI layer. Often times, a plateau is observed at about 0.5–0.6 V [6] but does not account for the entire observed irreversible capacity loss after the first cycle. This capacity loss can be as high as 30% of the first charge capacity, whereas the capacity of the plateau can account for <10%. The rest of the irreversible capacity loss has been attributed to loss of contact of the active material after the large volume change in the first charge [3].

By using silicon structured in the form of nanowires, we have shown that high capacities can be obtained and maintained for several cycles [17]. Analysis of the silicon nanowire electrodes showed that the nanowires did not pulverize during cycling. Thus, irreversible capacity loss due to lost or disconnected material seems unlikely in our case, but rather may be due to side reactions and SEI formation. For high surface area materials such as nanowires, we can expect a higher reactivity of the electrode with the electrolyte, which may have implications for long term cycling, depending on which species are being formed.

* Corresponding author. Tel.: +1 650 723 4613; fax: +1 650 725 4034.
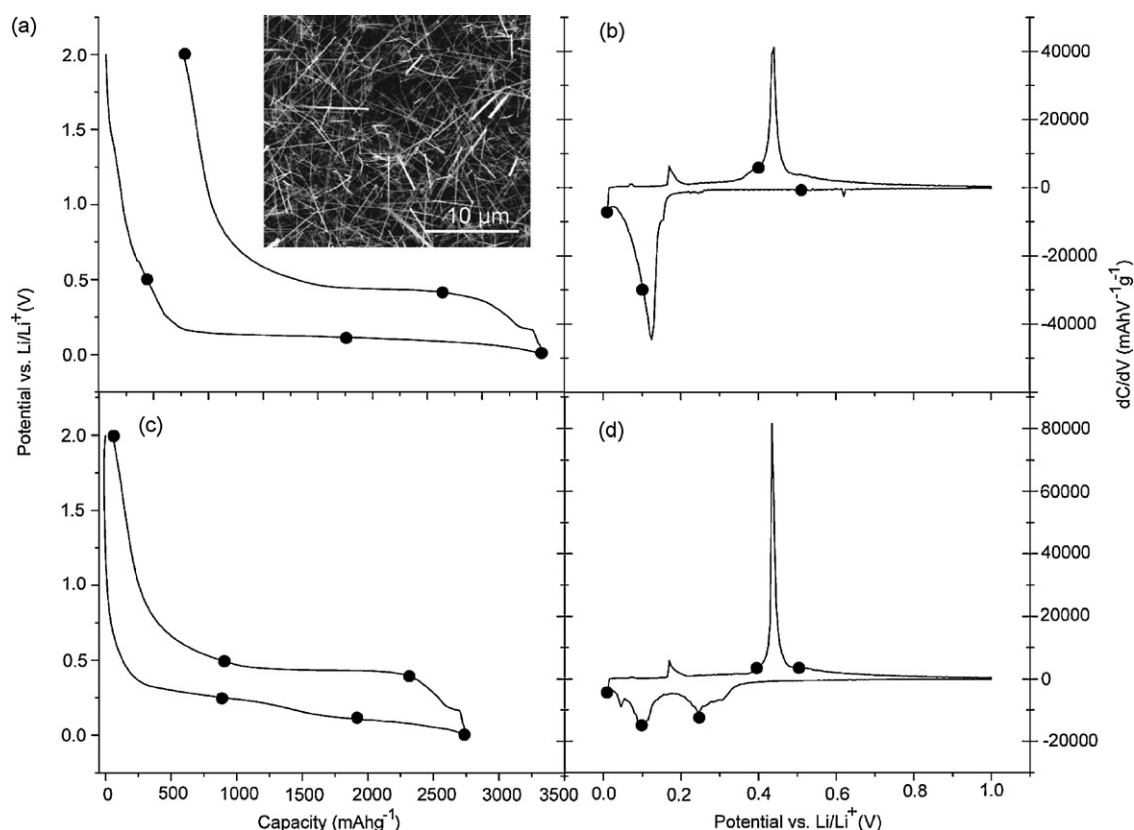 E-mail address: yicui@stanford.edu (Y. Cui).

Fig. 1. Galvanostatic voltage profile (a) and differential capacity curve obtained from electrochemical potential spectroscopy (b) for the first lithium insertion process into the SiNWs. (c) and (d) show the data for the second cycle. The black dots mark the potentials at which samples were made for XPS and SEM analysis. The inset shows an SEM image of the SiNWs.

Here we report our study on the SEI formation on the surface of SiNW electrodes using X-ray photoelectron spectroscopy (XPS), scanning electron microscopy (SEM), and electrochemical impedance spectroscopy (EIS). To our knowledge, this is the first study of this kind on crystalline Si nanowire electrodes, although the SEI layer formation has been studied on amorphous Si thin films [18,19] and particles [20]. We have focused on the first two cycles to study the formation reactions that occur in the very beginning of the cell operation in order to facilitate understanding of the origin of the large irreversible capacity loss commonly observed in silicon electrodes. We also will compare the SEI formation on our Si nanowire electrodes with work already reported for graphite and silicon [18–20]. We will also comment on the bonding environments and chemical states of the Si as analyzed from the Si 2p high resolution scans. Using the information learned from the SEI studies, we will also attempt to find the optimal experimental conditions for obtaining the best cycling performance.

2. Experimental

2.1. Sample preparation

The SiNW electrodes were prepared as discussed previously [17] by using a gold-catalyzed, vapour–liquid–solid growth directly onto stainless steel 304 substrates. The SiNW electrodes were assembled into aluminized polyethylene pouch "coffee bag" cells using a Celgard 3401 separator, 1 M $LiPF_6$ 1:1 (v/v) ethylene carbonate:diethylcarbonate (Ferro) electrolyte, and Li foil as the counter electrode. Several samples were made and cycled to different states of charge or discharge vs. Li/Li^+ (Fig. 1) using galvanostatic measurements with a 0.05C rate using a Maccor 4300 tester: in the first charge, 0.5, 0.1 V, and 10 mV (fully charged); then 0.4 V in the

discharge and 2.0 V (fully discharged). For the second cycle, samples were prepared with charge to 0.1 V and 10 mV, and discharge to 0.4, 0.5, and 2.0 V. After the desired state of charge or depth of discharge was obtained, the samples were washed in dimethyl-carbonate overnight to remove excess electrolyte. The morphology of the surface films and SiNWs were characterized using scanning electron microscopy (FEI XL30 Sirion).

2.2. X-ray photoelectron spectroscopy

XPS analysis of the surface was conducted with a PHI 5000 VersaProbe (Physical Electronics, Chanhassen, MN) equipped with an Al Kα X-ray radiation source. The samples were transferred to the XPS sample chamber using an Ar-filled transfer bag with no direct contact to air. The X-ray takeoff angle was 45° and the spot size was about 200 μm. No charge neutralization was used. The survey scans were taken with an energy resolution of 1.0 eV using a source with power and current of 125 kW and 10 μA, respectively. Depth profiling was performed by sputtering using an Ar^+ ion beam with a beam energy of 1 kV and beam current of 0.5 μA. Survey scans and high resolution scans of the Si 2p, C 1s, O 1s, F 1s, Li 1s, and P 2p energy spectra were taken of each sample to identify the compounds present on the surface. The high resolution scans were obtained with a pass-energy of 23.5 eV and energy resolution of 0.1 eV. The spectra were calibrated to the hydrocarbon peak at 284.5 eV.

The molecular composition of the SEI layer was determined by analyzing the XPS high resolution scans. The peaks were assigned according to assignments made by other SEI studies on graphite electrodes [14,21,22]. For the C 1s spectrum, the binding energy for hydrocarbons was assigned to 284.8 eV; polyethylene oxide (PEO)-type oligomers with a structure of $-(CH_2CH_2O)_n-$ were

assigned to 286.5 eV; lithium carbonate (Li_2CO_3) was assigned to 290 eV; lithium alkyl carbonates ($R–CH_2OCO_2Li$) and lithium ethers ($R–CH_2OLi$) were assigned to 288 eV and distinguished by different O 1s peaks. In the O 1s spectrum, the oxygen signal from the PEO-type oligomers was assigned to 533 eV; the Li_2CO_3 was assigned to 532 eV; the lithium alkyl carbonates were assigned to 533.5 eV; the lithium ethers were assigned to 532 eV. In the F 1s spectrum, lithium fluoride (LiF) was observed at 685 eV while the P–F bond from $LiPF_6$ was found at 687 eV. The P–F bond from $LiPF_6$ was also observed in the P 2p spectrum at 136 eV while lithium-containing phosphates ($Li_xPF_yO_z$) were observed at 134 eV.

2.3. Electrochemical impedance spectroscopy

For electrochemical impedance spectroscopy measurements, a three-electrode cell geometry [23] was used. The explored frequency range was from 50 kHz to 100 mHz under 10 mV of amplitude and no bias voltage was applied. Measurements were performed after the cell was allowed to equilibrate to the open circuit voltage for 15 h at different states of charge or discharge. The impedance measurements were conducted with a Bio-Logic VMP3 multi-channel galvanostat-potentiostat.

3. Results and discussion

3.1. Electrochemical results

The voltage profile and differential capacity results are shown in Fig. 1a and b for the first cycle and Fig. 1c and d for the second cycle. The inset in Fig. 1a shows a SEM image of the pristine SiNWs before lithiation. The small peak at ∼0.6 V in the differential capacity curve of the first cycle (Fig. 1b) has been traditionally attributed to SEI formation on Si electrodes [6]. As the potential is decreased, there is little current until lithiation of the Si begins at about 0.1 V. The predetermined voltage cutoffs used for the samples are indicated by the points in Fig. 1.

3.2. XPS results

For each sample, the atomic percents of the elements present on the surface were determined using a survey scan obtained from XPS. This data is shown in Fig. 2a. The distribution of the elements varies for each sample, suggesting that the SEI layer is dynamic over the voltage range. The signal from the Si disappears at 0.1 V in the first charge, indicating that the SEI layer has grown thicker than the XPS penetration depth (∼10 nm). This confirms that SEI formation is not limited to the region at 0.6 V as previously thought, but rather occurs in parallel with Li insertion at lower potentials. From our previous data [17], this does not appear to affect the cyclability of the SiNW electrode. This is different from graphite electrodes, Li-ion insertion can be obstructed if good, passivating surface layers are not formed at potentials higher than lithium intercalation [10,11].

3.2.1. SEI composition

During the first charge, the SiNWs are slowly polarized to low potentials using galvanostatic charging. As in graphite electrodes [12], this results in a gradual, voltage dependent formation of the SEI layer. Fig. 2b shows a summary of the composition of the surface of each sample as determined by identifying the compounds based on peaks from the high resolution spectra.

In the first charge to 0.5 V, the SEI layer is composed almost equally of hydrocarbons, PEO-type oligomers, LiF, Li_xPF_y and $Li_xPF_yO_z$ products, with smaller amounts of lithium alkyl carbonates and ethers. These species are consistent with previous studies and are the main reduction products observed in this electrolyte [15,16,21,24]. The carbonate solvent can be reduced to form lithium
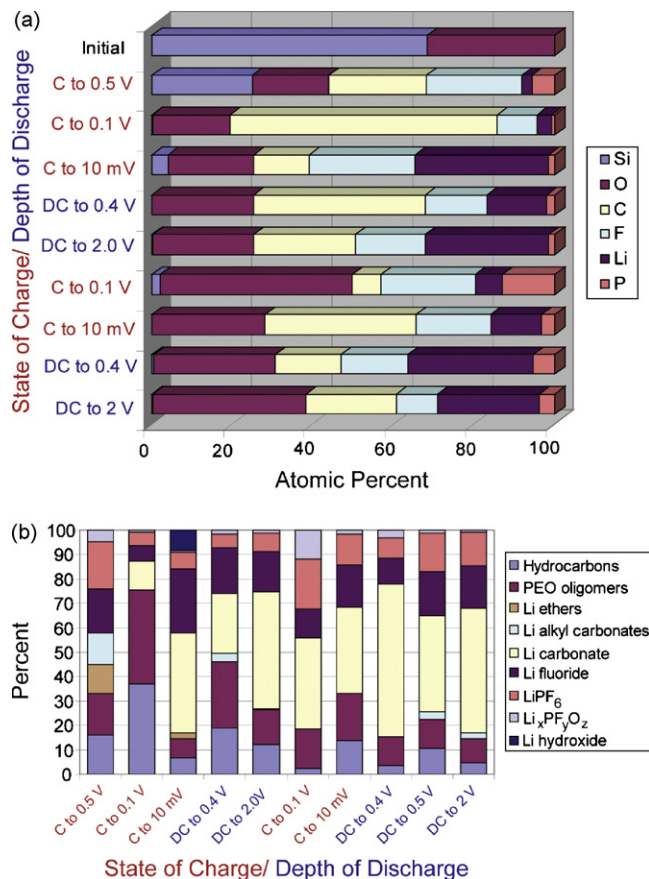

Fig. 2. (a) Surface composition of the SiNW samples as derived from the XPS survey scan. The atomic percentages are shown for different potentials during the charge and discharge. (b) Molecular species found on the surface of the SiNW samples at different potentials as determined from the XPS high resolution scans.

alkyl carbonates and ethylene gas, which can further polymerize into hydrocarbons or form PEO-containing oligomers. The linear diethyl carbonate can also be reduced to lithium ethers. The $LiPF_6$ salt can react with impurities such as HF and H_2O to form Li_xPF_y and $Li_xPF_yO_z$ like products, as well as LiF. LiF can also be formed from the decomposition of $LiPF_6$, which is unstable at low potentials.

In the first charge to 0.1 V, the SEI surface consisted predominately of hydrocarbons and PEO-oligomers, indicating that more electrolyte was being reduced. Li_2CO_3 was also observed but no Li alkyl carbonates or ethers were observed, suggesting that these less stable products transformed into Li_2CO_3. The amount of LiF and $LiPF_6$ was lower than at 0.5 V.

The atomic percents of the elements and high resolution spectra for the C 1s, O 1s, and F 1s peaks for the sample charged to 0.1 V are shown in Fig. 3 as a function of sputtering. The sputtering rate for the depth profile in Fig. 3b was determined to be 4 nm min^{-1} as measured on a SiO_2 reference. However, due to the inhomogeneous nature of the SEI layer, this sputter rate may not be entirely accurate and thus we only use it to estimate the surface layer thicknesses. Upon sputtering, the C–O features disappeared from the C 1s peak, suggesting that the hydrocarbons and PEO are part of an organic layer on the surface. $LiPF_6$ species were also found on the outer layer, with more LiF on the surface of the electrode. This is consistent with previous observations on Li and Li_xC electrodes, where the SEI is actually a mosaic consisting of an inorganic layer closer to the surface of the electrode with an organic, polymer containing layer at the interface with the electrolyte [14]. Sputtering also revealed Li_2O and LiOH features in the O 1s peak. These species have been
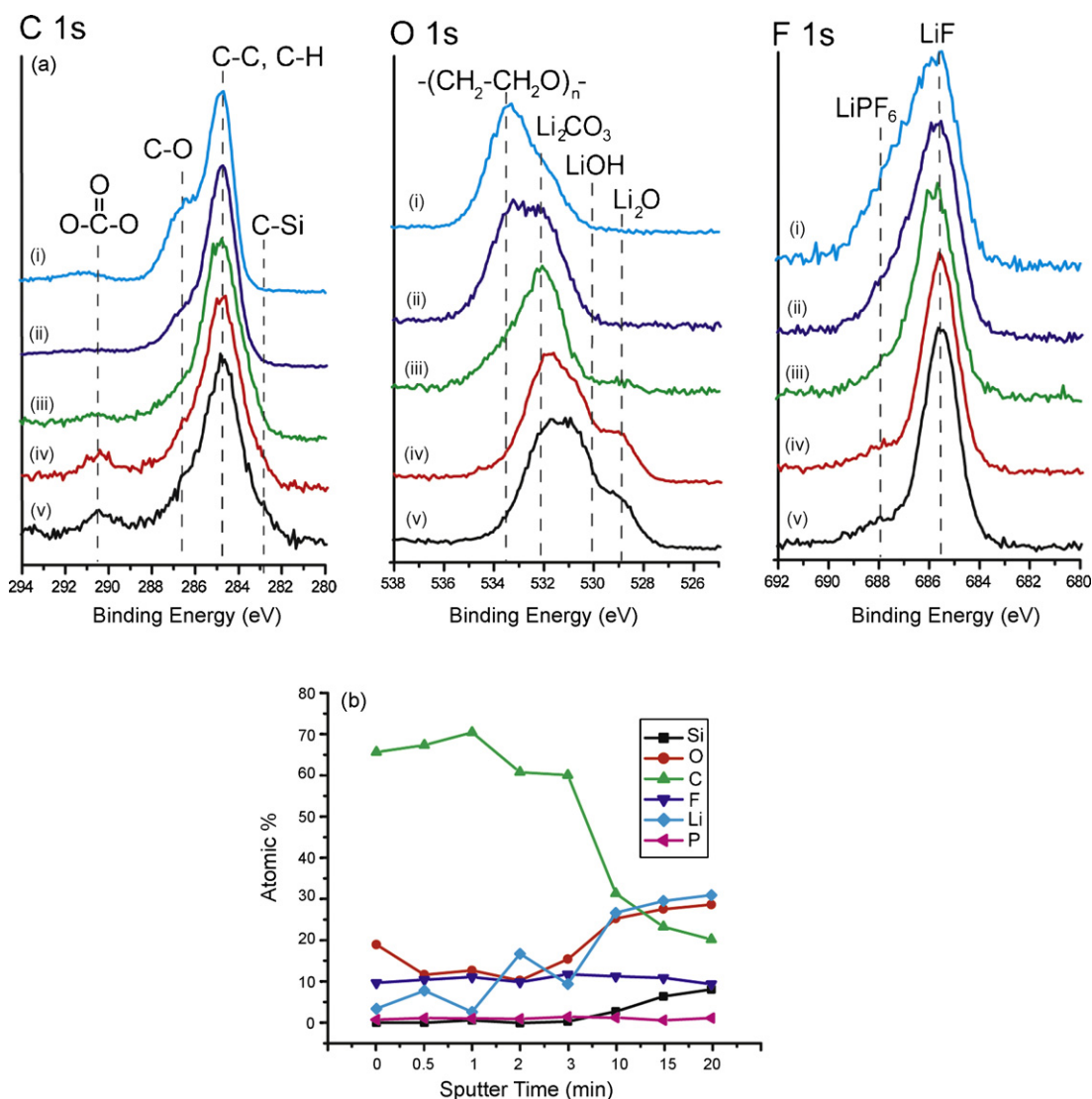
Fig. 3. (a) High resolution spectra for the C 1s, O 1s, and F 1s peaks for the SiNW sample charged to 0.1 V shown after different sputtering times. Using an approximate sputter rate of 4 nm min^{-1}, the thicknesses are (i) 0 nm (initial surface prior to sputtering), (ii) 2 nm, (iii) 12 nm, (iv) 60 nm, and (v) 80 nm. (b) Depth profile from SiNW sample charged to 0.1 V with an approximate sputter rate of 4 nm min^{-1}.

observed at the surface of graphite electrodes, but may also be due to a sputter-induced decomposition [14] of Li_2CO_3.

At the full charge to 10 mV, the SEI surface consisted mainly of Li_2CO_3 and LiF. The Li_2CO_3 is formed as a product of electrochemical reduction of the electrolyte, but the LiF is formed as a decomposition product rather than an electrochemical one. LiF can be formed from various mechanisms as discussed in the literature [21], which include reactions between $LiPF_6$, Li_2CO_3, HF, and/or water.

During the discharge, Li is removed from the amorphous Li_xSi nanowire to reveal amorphous Si nanowires [17]. We believe that the dealloying process may also leave the Si in a highly porous state. The SEI layer at 0.4 V in the discharge was observed to have higher amounts of hydrocarbon and PEO-type oligomers than the fully charged sample. This may be due to the exposure of the electrode to fresh electrolyte during dealloying. LiF and Li_2CO_3 remained the major components of the SEI at this potential.

At the full discharge to 2 V, the SEI was found to be composed predominately of Li_2CO_3, with other major species being LiF and $LiPF_6$. In the second cycle, the composition remained the same both during the charge and discharge. This suggests that the compositional formation of the SEI is an important feature during the first cycle and afterwards stays mostly the same, with Li_2CO_3 as the

major species. This in contrast to work done on amorphous Si thin films [18], where LiF was found to be the main component of the SEI. While the reason for this difference is currently not clear, it is possible that the higher surface area of the SiNWs may play a role.

3.3. SEI morphology

Previous SEM analysis of the SEI formed on amorphous Si thin film electrodes [18,19] at different states of charging and discharging revealed several key points. First, the morphology of the surface film changes drastically during cycling. The initial flat layer becomes rougher until it appears to be covered in a film composed of nanometer to micron sized particles. At the full state of charge as well as during the discharge, cracks can be observed in the films due to volume expansion of the Si layer beneath it. The SEM characterization is complicated by the fact it is difficult to visually distinguish the amorphous Si thin films from the SEI layer. In our case, the characteristic shape of the nanowires facilitates the differentiation between the morphology changes of the Si and of the SEI layer itself.

SEM observation of the SiNW samples at different points of charge and discharge confirmed that the surface layer changes as a function of the potential. The pristine SiNWs are characterized
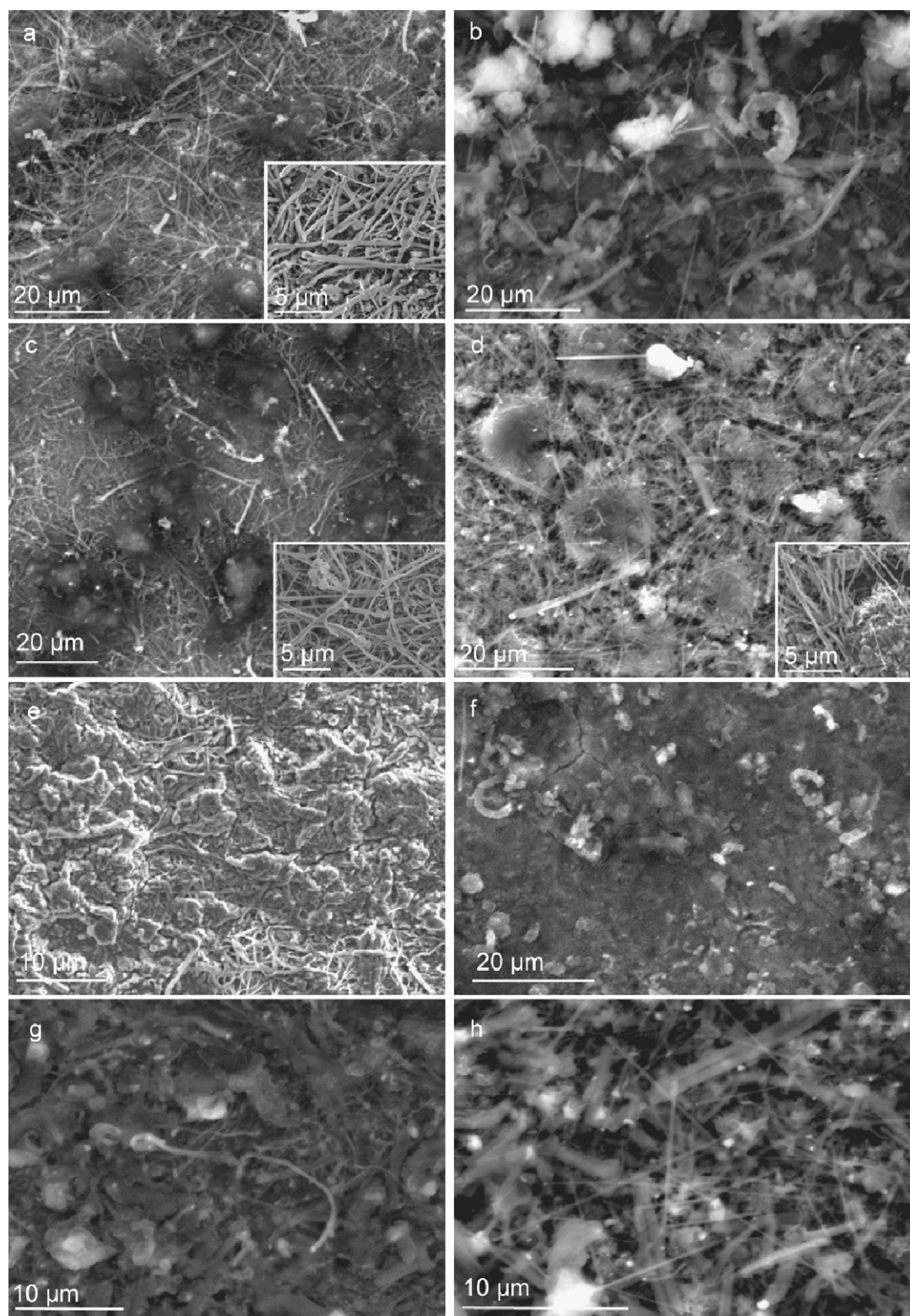
Fig. 4. SEM images of SiNWs and SEI layer at different potentials: the first charge to (a) 0.1 V and (b) 10 mV; the first discharge to (c) 0.4 V and (d) 2.0 V; the second charge to (e) 0.1 V and (f) 10 mV; the second discharge to (g) 0.4 V and (h) 2.0 V.

by clean surfaces and sharp boundaries (Fig. 1a, inset). In contrast, after the SiNWs had been charged to 0.1 V, the surfaces of the NWs were no longer smooth but rather rough in appearance due to what appears to be a conformal coating (Fig. 4a, inset). On the surface of the NW network, there also appeared to be regions covered with deposits of SEI products. From the sputter profile, it

was estimated that the layer covering the NWs was about 40 nm thick.

Further charging to 10 mV (Fig. 4b) revealed a very different type of film that consisted of a composite of different kinds of particles and deposits. Many of the particles are covering the SiNWs, but some are found adjacent to the NWs. The location of these deposits
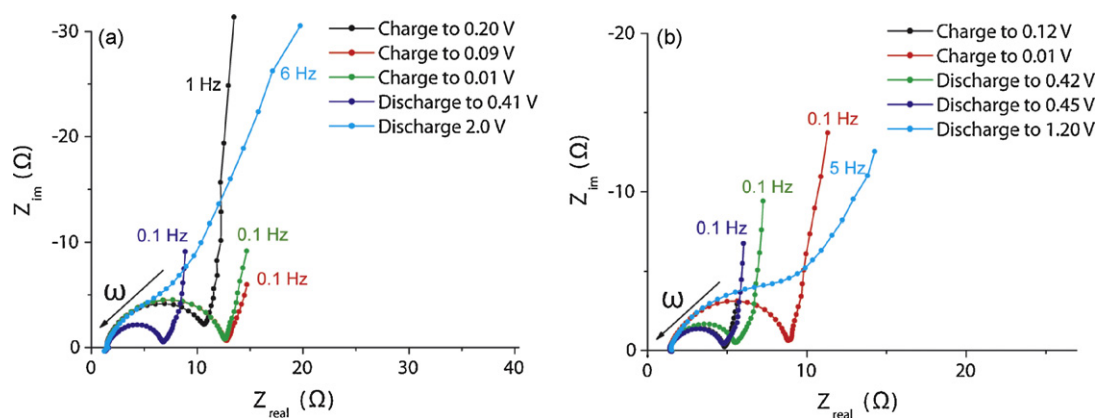
Fig. 5. Nyquist plots of the SiNW samples at different potentials of the (a) first and (b) second cycle.

suggests that there is deposition on or close to the substrate and growth outwards. Because the NW layer can be considered a highly porous film rather than a planar solid, it is possible that SEI products can form on the substrate itself between adjacent NWs. This may particularly be the case for electrochemical reduction products, since the metallic current collector is more conducting than the SiNWs, making it a preferential nucleation site for the formation of these species.

During the discharge, the large particles were no longer present, suggesting partial dissolution of the SEI layer. Surprisingly, at 0.4 V in the discharge (Fig. 4c), the SiNW network looks almost identical in morphology observed at 0.1 V in the charge (Fig. 4a). A similar dissolution of the SEI during the discharge has been observed in graphite electrodes using XPS and atomic force microscopy (AFM) imaging [21]. At the discharge to 2 V, the morphology of the film looks very different (Fig. 4d). Instead of appearing like a cohesive film consisting of both particles and NWs, the film appears to be broken up, with the particles residing as islands separated from the NWs (Fig. 4d, inset). Additionally, the NWs look more separated from each other and appear to have less of a surface coating as seen from the higher Si signal in the survey scans at 2 V than at 0.4 V in the discharge (Fig. 2a). These observations suggest that the SEI film may have further dissolved during the discharge to 2 V. We emphasize here that the NWs themselves do not appear to have pulverized. Although we do observe cracks in the film as well, it is clear that this is due to the SEI layer, and not the SiNW active material.

During the second charge, the SEI film has reformed on the surface of the SiNWs at 0.1 V (Fig. 4e). The film appears thicker than in the first cycle, indicating that the SEI growth still plays a large role after the first cycle. At further charging to 10 mV, the SEI has almost completely covered the NWs (Fig. 4f). During the discharge, more of the NWs are visible at 0.4 and 2 V (Fig. 4 g and 4 h, respectively), indicating that the SEI film is indeed dissolving.

Electrochemical impedance spectroscopy and galvanostatic measurements were used to determine how the morphological changes of the SEI may affect the performance of the SiNW cycling. Fig. 5 shows the Nyquist plots at different states of charge and depths of discharge. In the first cycle (Fig. 5a), the surface impedance [25] decreases with the state of charge, indicating that the coverage of the SiNWs with the SEI film results in better charge transfer. This may be due to the large amount of Li_2CO_3 on the surface, which has been known to play an important role as a passivating, low impedance layer in Li metal and Li_xC electrodes [12]. However, during the discharge, the impedance increases drastically at 2 V where the SEI layer has partially dissolved. This suggests that a cohesive SEI layer is necessary for low impedance in the SiNW electrode. Analysis at 1.2 V in the discharge of the second cycle

(Fig. 5b) also showed a large impedance, indicating that an optimal discharge voltage should reside between 0.4 and 1.2 V.

To test this, galvanostatic cycling at the 0.2C rate with different discharge voltage cutoffs were compared to evaluate the effect on long-term cycling stability. Fig. 6 shows the capacity vs. cycle number for SiNWs cycled between a 70 mV charge and 0.7 V discharge compared with cycling between 70 mV and 2 V. Initially, for the 0.7 V cutoff, the capacity is lower, indicating the SiNWs are not fully delithiated. However, after about 40 cycles the performance using the 0.7 V cutoff is improved. For long term cycling stability, it may be important for the SEI morphology to remain relatively constant. Repeated formation and dissolution of species around the active material may be detrimental to good Li diffusion and kinetics because of the constantly changing interfaces. Therefore, it may be better to avoid exposing the electrode to potentials that may promote large changes in SEI morphology. This was also confirmed by charging to 10 mV and discharging to 2 V. As shown in Fig. 6, using these extreme voltage cutoffs resulted in faster capacity loss than using the other cutoffs.

3.4. Silicon structure and bonding

The XPS spectrum of the as grown-SiNWs is shown in Fig. 7. It is characterized by the Si–Si peak at 99 eV and the Si–O peak at about 103 eV due to SiO_2. The presence of the native oxide is due to the
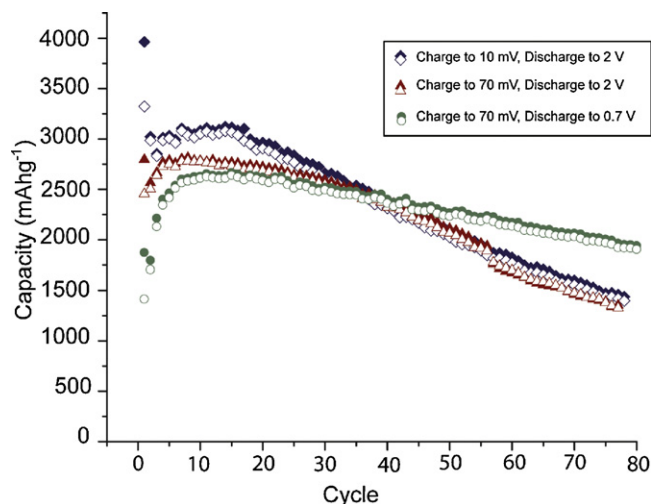

Fig. 6. Capacity vs. cycle number for galvanostatic cycling of SiNWs at the 0.2C rate using different voltage cutoffs: charge to 10 mV and discharge to 2 V (diamonds), charge to 70 mV and discharge to 2 V (triangles), and charge to 70 mV and discharge to 0.7 V (squares). The solid figures are the charge capacities and the open figures are the discharge capacities.
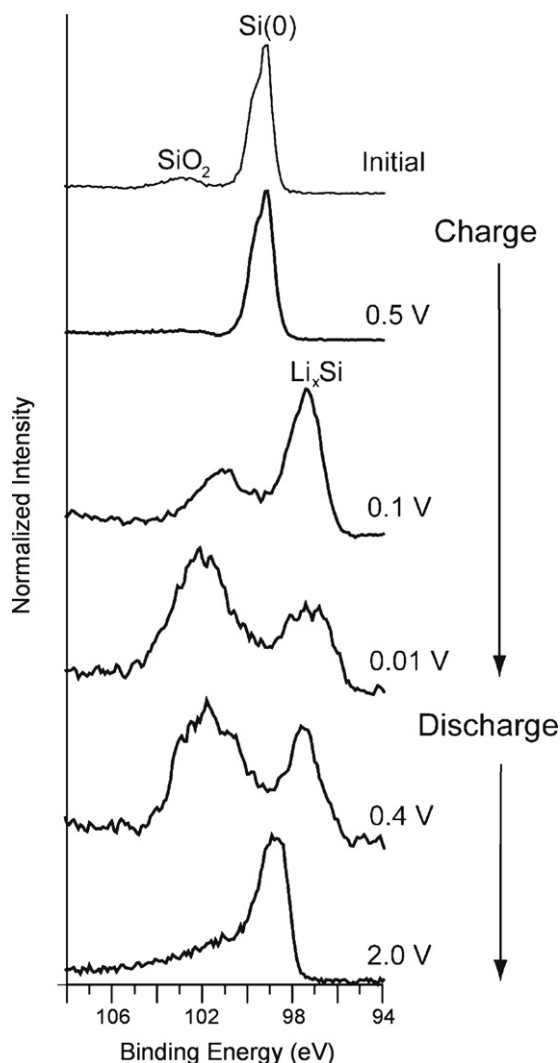
Fig. 7. XPS high resolution spectra of Si 2p peak of SiNWs at different potentials during the first cycle.

SiNWs being exposed to air after the growth, which results in the formation of 1–3 nm SiO_2 on the surface [26].

After charge to 0.5 V, analysis of the Si 2p peak shows that the native oxide has been removed. At 0.5 V charge, no Li insertion has begun, so the Si is still in the zero oxidation state as observed by the peak centered at 99 eV. There are two possibilities for the removal of the native SiO_2. The native oxide could be electrochemically removed using the reaction $4Li + SiO_2 \rightarrow 2Li_2O + Si$. Alternatively, it could be chemically removed by hydrofluoric acid in the electrolyte, which is present either as impurities or formed in situ due to the decomposition of $LiPF_6$. Because features indicative of Li_2O were not observed in the O 1 s peak, we are inclined to believe that the native oxide was not electrochemically reduced, but further investigation of this matter would be beneficial.

At 0.1 V charge, the Si 2p peak was observed to shift to lower binding energies, indicating it is in a reduced state due to alloying with Li [18]. The peak observed at around 101 eV may be due to Si bonding to carbonaceous species, as supported by the shoulder in the C 1s peak at higher binding energies (Fig. 3). Thus, we believe that Si bonding to the SEI layer is through carbon and not oxygen.

At the full charge to 10 mV, the high-resolution scan of the Si 2p surface showed two different environments for the Si. The peak due to Si bonding to the SEI became broader and shifted to higher energies, suggesting that there is Si is bonded to many species, including carbon, oxygen and possibly fluorine [19,27]. The peak at 98 eV representing the Si alloyed with Li was also present, but the peak area was smaller than that for Si bonded to the SEI. Based on our previous SEM and TEM observations [17], at the end of the charge, the NWs are completely amorphous and have increased in diameter and in length. The NWs also have a heavily textured surface and appear to increase in porosity. These characteristics may coincide with an increase in surface area, which allows for the exposure of more Si on the surface to bond with SEI and electrolyte. Due to the high surface to volume ratio of the NWs, it appears that surface bonding plays a large role in the bonding of the Si compared to Li alloy formation in the bulk of the NW.

Analysis of the Si 2p peak at 0.4 V in the discharge showed a similar set of environments as observed at the fully charged state. Because only about a quarter of the Li has been removed at 0.4 V, the Si is still highly lithiated. At the fully discharged state at 2 V, the Si 2p main peak was observed at 99 eV, indicating that the Si was no longer in the reduced state alloyed with Li, but was instead close to the its original Si(0) state. The shoulder of the peak towards higher energies suggests that there were still some surface species bonded to the Si.

3.4.1. Native oxide

Very little work has been done investigating the effect of the presence of the native oxide found on silicon on the cycling performance. Most silicon samples, even if prepared under vacuum from e-beam evaporation or sputtering, are eventually exposed to air during which oxide formation can occur. The large irreversible capacity of 41% observed in silicon nanocrystals [6] was attributed to the electrochemical reduction of the SiO_2 by lithium. Because of the large surface area of the nanocrystals, there was a large amount of SiO_2 present, which would presumably result in a large irreversible capacity loss in the first cycle.

Using the same reasoning, a similar phenomenon should be expected in the SiNWs. However, we have found that after charging to 0.5 V in the first cycle, the native oxide has already been removed (Fig. 7). Moreover, the capacity at this potential is very small ($\sim$100 mAh g^{-1}) and cannot account for all of the irreversible capacity loss. Therefore, we do not believe the native oxide is the cause of the large irreversible capacity loss commonly observed in Si electrodes.

Nonetheless, removing the native oxide beforehand should give valuable insights into its role in the surface chemistry of the SiNWs. To remove the native oxide, the SiNWs were immersed in 5% hydrofluoric acid and heated on a hotplate at 110 °C inside an Ar-filled glovebox to remove the water. After etching with hydrofluoric acid, the NW is terminated with Si–H bonds [26]. After etching, a sample of SiNWs was immersed into the electrolyte for several minutes, then rinsed with dimethyl carbonate and analyzed using XPS. Because the ⟨1 1 1⟩ is the main growth direction for SiNWs, the ⟨1 0 0⟩ plane is the surface exposed to the electrolyte. Therefore, as a comparison, a Si ⟨1 0 0⟩ wafer was etched and prepared in a similar manner.

XPS analysis of the Si ⟨1 0 0⟩ wafer found the common reduction products of the electrolyte on the surface, including hydrocarbons, PEO-type oligomers, Li alkyl carbonates, LiF, and $LiPF_xO_y$ (Fig. 8a). This suggests that the electrolyte was chemically reduced by the reactive Si–H bond. The high resolution scan of the Si 2p peak showed that Si was present in the Si(0) state, but there was also Si bonded to oxygen and carbon containing species as observed from the peak at higher binding energies (Fig. 8b).

Analysis of the SiNWs showed a very different surface (Fig. 8a and b). First, no Si signal was observed in the initial survey scan, indicating the SiNWs were buried underneath greater than 10 nm of SEI layer. The Si signal was revealed using sputtering. As with
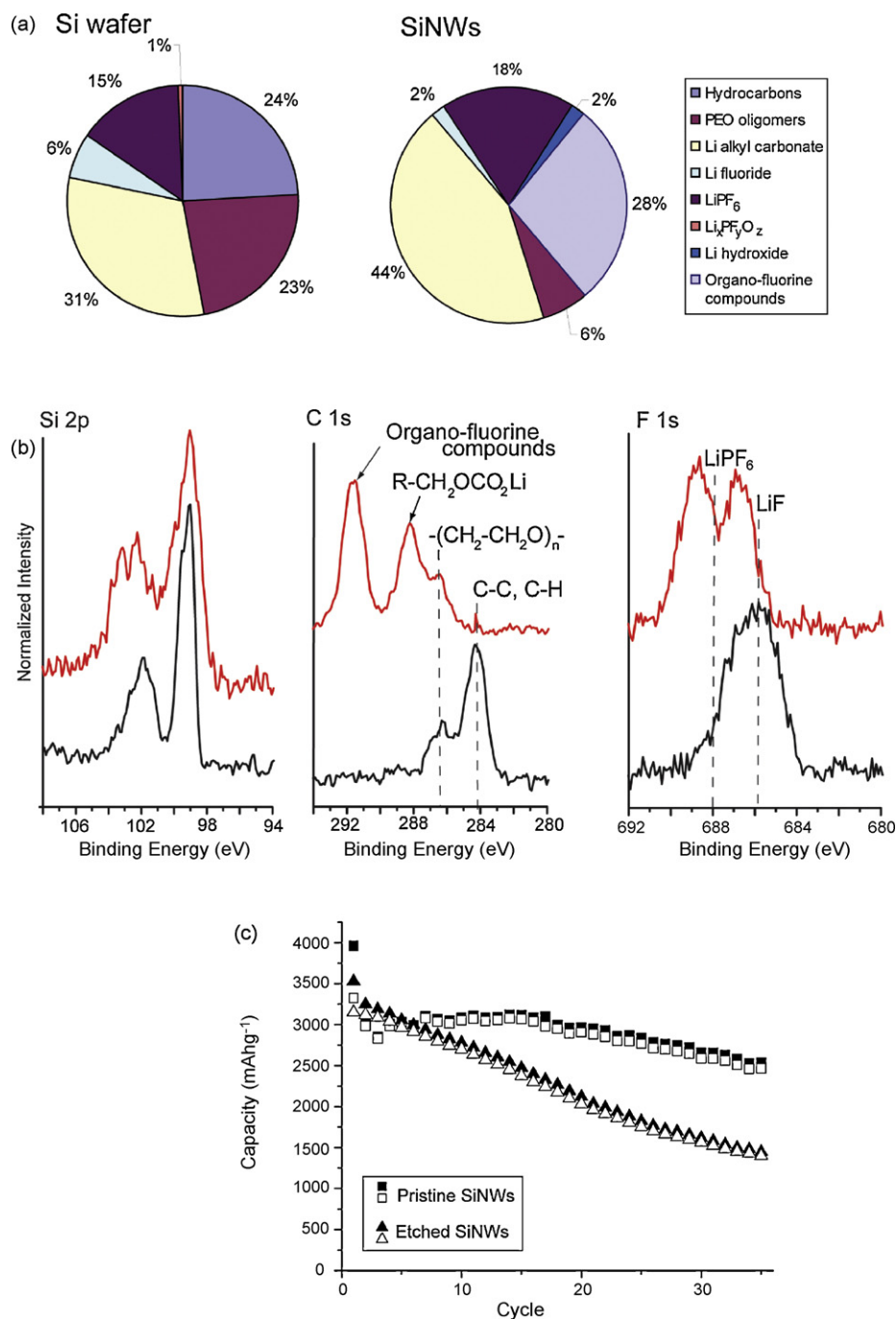
Fig. 8. Results of HF etching (a) Surface composition as determined by XPS, (b) XPS high resolution spectra of Si 2p, C 1s, and F 1s for the Si wafer (black) and SiNWs (red), (c) capacity vs. cycle number for galvanostatic cycling of HF-etched SiNWs and pristine SiNWs (un-etched) at the 0.2C rate. The solid figures are the charge capacities and the open figures are the discharge capacities. (For interpretation of the references to color in this figure legend, the reader is referred to the web version of the article.)

the Si wafer, the Si was also present in the Si(0) state as well as bonded to other species. However, the high energy peak was broader and extended out to 105 eV, suggesting the presence of Si–F bonds. In the C 1s peak, C–F bonds were also observed by the prominent peak at 292 eV. The new peak observed at about 689 eV suggests O–F bonds. This may signify the presence of fluorine-containing organic species [22] formed on the surface of the SiNWs. The other main species observed were attributed to Li alkyl carbonates and $LiPF_6$. The difference between the surface chemistry of the etched SiNWs and Si wafer may be due to the increased surface area of the SiNWs leading to higher reactivity with the electrolyte.

To test the effect of the different surface chemistry on the cycling performance, a sample of SiNWs was etched with hydrofluoric acid and assembled into a cell as described previously. The capacity vs. cycling results are shown in Fig. 8c for the etched SiNW sample compared with a sample that was not etched (pristine SiNWs). The efficiency in the first cycle was slightly improved by removing the native oxide, with 89% coulombic efficiency in the etched sample and 76% in the un-etched sample. However, this suggests that reduction of the native SiO_2 is not the sole contributor to the irreversible capacity loss in the first cycle. It is likely that most of the capacity loss is due to SEI formation from the decomposition of the electrolyte. Galvanostatic cycling of the SiNWs using the 0.2C

rate showed that the etched samples had much worse performance, losing more than half the initial capacity in only 35 cycles. Because the native oxide was observed to be removed in the regular sample at 0.5 V charging anyways (Fig. 7), the presence or absence of the SiO_2 in the initial stage does not seem to be important for deciding the long-term cyclability of the electrode. Rather, what is important is the surface film formed on the SiNWs. In the case of the SiNWs etched with hydrofluoric acid, the highly reactive Si–H bonds on the surface formed a different surface layer with the electrolyte, one that was composed predominately of organo-fluorine compounds. In the regular sample, however, the native oxide allowed the Si surface to remain passivated and only form the common electrochemically derived reduction products on the surface.

4. Conclusions

We have characterized the nature of the SEI layer formed on SiNW anodes using the 1 M $LiPF_6$ EC:DEC electrolyte. It is clear that a great deal of the SEI formation occurs at potentials where Li insertion into the Si is also taking place. The fact that the Si expands in volume at the same time also contributes to the dynamic nature of the SEI film. The morphology of the SEI was found to be voltage-dependent, with a thick layer consisting of large particles forming at low potentials, which partially dissolves and forms cracks as the potential is increased in the discharge. Improved cycling performance was observed when tuning the voltage cutoffs to avoid large changes in SEI morphology, suggesting that the cycle life in SiNWs may rely a great deal on the SEI layer. This may be due to the enhanced reactivity of SiNWs due to the large surface area, as well as the composition of SEI products formed on the surface of the nanowire. Thus, it will be beneficial to explore different electrolytes and additives to determine the optimal SEI layer for long-term cycling.

Acknowledgements

References

[1] G.-A. Nazri, G. Pistoia, Lithium Batteries: Science and Technology, Kluwer Academic/Plenum, Boston, 2004.
[2] M. Green, E. Fielder, B. Scrosati, M. Wachtler, J.S. Moreno, Electrochem. Solid-State Lett. 6 (2003) A75–A79.
[3] J.H. Ryu, J.W. Kim, Y.-E. Sung, S.M. Oh, Electrochem. Solid-State Lett. 7 (2004) A306–A309.
[4] T. Takamura, S. Ohara, M. Uehara, J. Suzuki, K. Sekine, J. Power Sources 129 (2004) 96–100.
[5] M.N. Obrovac, L.J. Krause, J. Electrochem. Soc. 154 (2007) A103–A108.
[6] J. Graetz, C.C. Ahn, R. Yazami, B. Fultz, Electrochem. Solid-State Lett. 6 (2003) A194–A197.
[7] T.D. Hatchard, J.R. Dahn, J. Electrochem. Soc. 151 (2004) A838–A842.
[8] B.A. Boukamp, G.C. Lesh, R.A. Huggins, J. Electrochem. Soc. 128 (1981) 725–729.
[9] E. Peled, J. Electrochem. Soc. 126 (1979) 2047–2051.
[10] D. Aurbach, B. Markovsky, I. Weissman, E. Levi, Y. Ein-Eli, Electrochim. Acta 45 (1999) 67–86.
[11] J.S. Gnanaraj, R.W. Thompson, J.F. DiCarlo, K.M. Abraham, J. Electrochem. Soc. 154 (2007) A185–A191.
[12] D. Aurbach, B. Markovsky, M.D. Levi, A. Schechter, M. Moshkovich, Y. Cohen, J. Power Sources 81–82 (1999) 95–111.
[13] A. Andersson, A. Henningson, H. Siegbahn, U. Jansson, K. Edstrom, J. Power Sources 119–121 (2003) 522–527.
[14] K. Edstrom, M. Herstedt, D.P. Abraham, J. Power Sources 153 (2006) 380–384.
[15] P.B. Balbuna, Y. Wang, Lithium-Ion Batteries: Solid-Electrolyte Interphase, Imperial College Press, London, 2004.
[16] D. Aurbach, Y. Gofer, in: D. Aurbach (Ed.), Nonaqueous Electrochemistry, Marcel Dekker, New York, 1999, pp. 137–212.
[17] C.K. Chan, H. Peng, G. Liu, K. McIlwrath, X.F. Zhang, Y. Cui, Nat. Nanotechnol. 3 (2008) 31–35.
[18] Y.M. Lee, J.Y. Lee, H.-T. Shim, J.K. Lee, J.-K. Park, J. Electrochem. Soc. 154 (2007) A515–A519.
[19] N.-S. Choi, K.H. Yew, K.Y. Lee, M. Sung, H. Kim, S. Kodambaka, J. Power Sources 161 (2006) 1254–1259.
[20] Y.-C. Yen, S.-C. Chao, H.-C. Wu, N.-L. Wu, J. Electrochem. Soc. 156 (2009) A95–A102.
[21] S. Leroy, F. Blanchard, R. Dedryvere, H. Martinez, B. Carre, D. Lemordant, D. Gonbeau, Surf. Interface Anal. 37 (2005) 773–781.
[22] H. Bryngelsson, M. Stjerndahl, T. Gustafsson, K. Edstrom, J. Power Sources 174 (2007) 970–975.
[23] M. Dolle, F. Orsini, A.S. Gozdz, J.-M. Tarascon, J. Electrochem. Soc. 148 (2001) A851–A857.
[24] A. Xiao, W. Li, B.L. Lucht, J. Power Sources 162 (2006) 1282–1288.
[25] E. Barsoukov, in: E. Barsoukov, J.R. MacDonald (Eds.), Impedance Spectroscopy: Theory Experiment and Applications, 2 ed., John Wiley & Sons, Inc., Hoboken, NJ, 2005, pp. 430–462.
[26] D.D.D. Ma, C.S. Lee, F.C.K. Au, S.Y. Tong, S.T. Lee, Science 29 (2003) 1874–1877.
[27] P. Ram, J. Singh, T.R. Ramamohan, S. Venkatachalam, V.P. Sundarsingh, J. Mater. Sci. 32 (1997) 6305–6310.